AN EXPANDED MATHEMATICAL MODEL OF MAMMALIAN CELL CYCLE REGULATION IN RESPONSE TO VARIED CIRCADIAN RHYTHM AND DNA DAMAGE

By

Jordan Lee Rolsma

A capstone project submitted for Graduation with University Honors

May 06, 2021

University Honors
University of California, Riverside

APPROVED

Dr. Joshua Morgan
Department of Bioengineering

Dr. Richard Cardullo, Howard H Hays Jr. Chair
University Honors

ABSTRACT

The mammalian cell cycle is a complex system of molecular interactions that dictates cellular growth, proliferation and, by extension, a wide range of biological processes. The cell cycle may be temporarily or permanently halted by increased expression of the cyclin-dependent kinase inhibitors p16, p21 and p53 in response to DNA damage stress, as well as disrupted expression of BMAL1, a circadian rhythm protein responsible for regulation of the sleep-wake cycle and maintenance of homeostasis. Such impediments to cell cycle function contribute to the pathology of an extensive variety of severe aging-associated diseases. As such, there is significant incentive to understand the interactions among the key regulators of the mammalian cell cycle in order to better inform future treatment options. Prior research has yielded a plethora of computational models that have attempted to model the cell cycle; however, these models lack key molecular signaling events, are modeled over non-representative time scales, and are limited in terms of the methods of senescence inductance that are studied. Further, a decisive knowledge gap exists in that no successful attempts have been made to model the interactivity of BMAL1 and cyclin-dependent kinase inhibitors. This work features the novel integration of a BMAL1 circadian rhythm module and individual p16, p21, and p53 protein DNA damage modules into an established computational model of a cell cycle system, with preliminary demonstration of the impact of varying levels of DNA damage and circadian rhythm variation on the functionality of the cell cycle. Future expansion of this model is projected to enable advanced study of aging-associated diseases such as glaucoma in cooperation with data obtained from *in vitro* experimentation.

ACKNOWLEDGEMENTS

I would like to extend my sincerest gratitude to Dr. Joshua Morgan for his invaluable mentorship throughout my research career - this project would not have been possible without his constant encouragement and guidance. I also gratefully acknowledge the efforts of my laboratory colleagues and classmates, Himani Thakkar and Brittany Gilbert, in reconstructing the circadian rhythm module that has been generously provided to me to be implemented in my final project. I also thank Gladis Herrera-Berkowitz and the UCR Department of Undergraduate Education for aiding me in my professional and academic development through the Chancellor's Research Fellowship program. Last but certainly not least, I express my unending appreciation and admiration for my parents for all of their unconditional love, faith and support.

TABLE OF CONTENTS

INTRODUCTION

The mammalian cell cycle is characterized by a series of stages that regulate cell growth and division and is dependent on a broad range of intercellular and extracellular factors.[1,2] An aging cell is considered to be senescent when it has fully exited the cell cycle in response to stress, biochemical interactions or other environmental stimuli and is no longer capable of division. This halt of cell cycle activity is induced by increased expression of the tumor-suppressor proteins p53, p21 and p16, and is closely associated with pathological progression of aging-associated diseases including cancers and the deterioration of bone, cardiac and neurological tissue and other vital biological structures.[3] Similarly, mammalian cells may also enter into quiescence, a state of cellular dormancy that is comparable to the concept of "reversible" senescence.[4]

Circadian rhythm proteins are biochemical feedback loop molecules that generate the characteristic 24-hour oscillatory rhythm of the mammalian sleep-wake cycle and maintain homeostasis of temperature and metabolism.[5,6,7] In addition to the aforementioned regulatory roles, circadian rhythm proteins, particularly Brain and Muscle ARNT-Like 1 (BMAL1), have also been shown to regulate *in vivo* senescence in mammalian cells, though this concept is not as thoroughly studied in *in vitro* settings.[8]

In recent years, numerous computational models have been constructed to gain a deeper understanding of the interactions among regulatory molecules that govern this cycle and entrance into senescence and quiescence; however, these models are often oversimplified, do not exhibit reliable cyclical behavior over biologically relevant time intervals, or rely on DNA damage as a singular method of stress inductance.[9,10,11,12] Notably, no current systems exist to model the complex interactions between regulators of the cell cycle and circadian rhythm proteins.

To address these deficiencies, this project aims to serve as a preliminary attempt at construction of a reliable, improved computational model of the mammalian cell cycle that considers both DNA damage and circadian rhythm variation as factors contributing to cycle regulation and inductance of senescence and quiescence. Through the incorporation of p53, p16, p21 and BMAL1 into an existing model of cell cycle behavior, the groundwork has been laid for expansion of this *in silico* model to provide valuable insight into the cooperative roles of circadian rhythm proteins, DNA damage signals, growth factors and cell cycle regulators in the mammalian aging process. In the future, this hybrid model may be applied as a foundation of drug discovery advancements in treating aging-associated diseases that display molecular overlap with circadian rhythm dysfunction, including endocrine disorders, various cancers, and glaucoma, the leading cause of irreversible blindness in the United States.[13,14,15,16] In particular, this model is intended to be supplemented with future experimental in vitro data obtained from trabecular meshwork (TM) cells of the human eye to aid in validation of the previously unstudied hypothesis that the corticosteroid dexamethasone (DEX) reliably induces a glaucomatous phenotype characterized by TM cell population loss in a BMAL1/p53-dependent fashion.[17,18,19,20]

METHODOLOGY

Literature Review

A thorough literature search was conducted for online research articles and studies pertaining to the mammalian cell cycle, DNA damage, circadian rhythm and computational models of the aforementioned topics. Relevant literature published in English were selected from PubMed, MEDLINE and various scientific journals and applied to the development of signaling pathway diagrams and a cohesive MATLAB ordinary differential equation (ODE) solver-based computational model.

Cell Cycle Model Reconstruction and Optimization

Five mammalian cell cycle and circadian rhythm models of varying complexity were identified from a comprehensive literature search and individually replicated in separate scripts using MATLAB Version 2020b computational modeling software. All models were rendered with the ode45 solver for nonstiff differential equations, and will hereafter be referred to as the Abroudi, Conradie, Iwamoto, Weis and Geier models. After replication, the Weis model was not determined to be necessary for this project and was not utilized in the further development of a comprehensive cell cycle script.[12] The Iwamoto model, meanwhile, was found to be the equivalent of an early iteration of the Abroudi model, and was therefore only used for comparison purposes during the optimization phase.[11] The Abroudi model, the most complex system replicated in this project, contained 64 ODEs and 145 constants representing distinct molecular reactions implicated in both the mammalian cell cycle and the DNA damage stress response as it relates to the p53 tumor suppressor gene.[9] However, the cyclical behavior of the cell cycle components of this model were found to be unreliable and only the DNA damage

module was utilized in the synthesis of the final model. The original Conradie model, meanwhile, comprised 78 constants, 9 algebraic equations, 52 rate equations and 24 ODEs and provided the basic framework of the cell cycle from which the final model was synthesized.[10] The original Geier model consisted of 24 constants and 7 ODEs, and was partially replicated and expanded upon by laboratory colleagues Himani Thakkar and Brittany Gilbert.[21] For the purposes of this project, only the BMAL1 module was incorporated into the final model.

Tables 1, 2, 3, and **4** contain the 134 constants, 12 algebraic equations, 89 rate equations, and 39 ODE equations, respectively, that comprise the completed computational model. The construction of this model may be divided into a sequence of four critical components. The first of these was the reconstruction of the Conradie model in its entirety to obtain a functional representation of a mammalian cell cycle system that was cyclically responsive to initial system inputs over an interval of 50 hours. One significant deviation from the functional units supplied by the Conradie model was made to facilitate upstream troubleshooting and separate modeling of the G1 phase, or growth phase of the cell, from the S, G2 and M phases that are characterized by DNA replication and division of the cell (**Figure 1**).[22] To accomplish this, the FLAG variable of the Conradie model was replaced with a coded loop that solved the ODE in two solution steps: the ODE was solved for the G1 and S/G2/M parts of the cell cycle separately. After completion of the M-phase the cell was computationally "split" by division of the MASS and GM variables representing cellular mass and general machinery. Each ODE passed final values as initial conditions to the next ODE to ensure seamless transition from each integration to subsequent timesteps.

Next, two novel modules were formulated and integrated into the optimized Conradie model to incorporate the influence of p21 and p16, two proteins associated with the DNA

damage stress response. From literature review, it was determined that p21 may be incorporated into the framework of the Conradie model by its upstream inhibitory influence on the Cyclin E/Cdk2 and Cyclin A/Cdk2 complexes, key regulators of cell cycle progression; likewise, p16 may be similarly integrated by its upstream inhibitory influence on the regulatory Cyclin A/Cdk2 and Cyclin B/Cdk 2 complexes, as well as its tendency to promote synthesis of Rb, the retinoblastoma protein that binds to the transcriptional factor E2F to prevent advancement of the cell cycle (**Figure 2**).[23,24] To successfully integrate these components, two ODE equations for p21 and p16 were generated from the formulation of six new rate equations (labeled v66 through v71 in **Table 3**) encompassing the signaling behavior previously described and six corresponding new constants (labeled k100 through k105 in **Table 1**). The Conradie ODEs representing the Cyclin A/Cdk2, Cyclin B/Cdk2, Cyclin E/Cdk2 and E2F/Rb complexes were also altered to include the newly integrated parameters. Constant values were optimized by systematic variation and plotting of corresponding ODEs until desirable behavior was obtained.

Following integration of p16 and p21, a module containing p53, an additional DNA damage stress response protein, was transferred from the Abroudi model and integrated into the updated Conradie model. From literature review, it was determined that this protein may be integrated into the existing framework of the existing hybrid model via the upstream promotion of p21 expression (previously incorporated into the model as explained above) by p53 (**Figure 2**).[25] To integrate this module, 21 constants (highlighted in orange in **Table 1**) and 3 algebraic equations (labeled DDS, DSB and DEG in **Table 2** to represent DNA damage events) were added to the master model, with 13 new rate equations (labeled v53 through v65 in **Table 3**) formed from the compartmentalized ODE equations provided in the Abroudi model. These rate equations formed the basis of 7 additional ODE equations (labeled ATMp, iChk2p, aChk2p,

p53p, Mdm2p, IFp, and Gadd45ap in **Table 4**) reconstructed in the format of the Conradie hybrid model. As the Abroudi model employed axes scales that differed from those of the Conradie model, a multiplicative time factor of 187 was applied to all integrated Abroudi constants and the numerator terms of rate equations v60 and v62 to ensure homogeneity of plots.

Finally, the Geier BMAL1 module was integrated into the comprehensive model. From literature review, it was determined that this protein may be incorporated into the framework of the hybrid model through the upstream inhibition of p53 (previously incorporated into the model as explained above) by BMAL1 (**Figure 2**).[26] To integrate this module, 24 constants (highlighted in red in **Table 1**) were added to the master model, with 18 new rate equations (labeled v72 through v89 in **Table 3**) formed from the ODE equations provided in the Geier model. These rate equations formed the basis of 7 additional ODE equations (labeled BeWe1p - BeWe7p in **Table 4**) reconstructed in the format of the Conradie hybrid model.

E2FT = 5.0	FB = 2.0	FE = 25.0	GA = 0.3	GB = 1.0
GE = 0.0	HA = 0.5	HB = 1.0	HE = 0.5	J8 = 0.1
K10 = 5.0	K12 = 1.5	K2 = 20.0	K20 = 10.0	K21 = 1.0
K22 = 1.0	K23 = 1.0	K23a = 0.005	K25 = 1000.0	K25R = 10.0
K26 = 10000.0	K26R = 200.0	K2a = 0.05	K2aa = 1.0	K30 = 20.0
K4 = 40.0	K6 = 100.0	K6a = 10.0	K8 = 2.0	K8a = 0.1
LA = 3.0	LB = 5.0	LD = 3.3	LE = 5.0	PP1T = 1.0
RBT = 10.0	YB = 0..05	YE = 1.0	eps = 1.0	v1k16 = 0.25
v2k18 = 10.0	v7k24 = 1000.0	v8k24r = 10.0	v20J3 = 0.01	v20K3 = 140.0
v20K3a = 7.5	v21J4 = 0.01	v22K34 = 0.05	v23J31 = 0.01	v23K31 = 0.7
v24J32 = 0.01	v24K32 = 1.8	v26J13 = 0.005	v26K13 = 5.0	v27J14 = 0.005
v27K14 = 2.5	v31K27 = 0.2	v32K28 = 0.2	v33MU = 0.061	v34J15 = 0.1
v34k15 = 0.25	v35K11 = 1.5	v35K11a = 0.0	v36K29 = 0.05	v37K33 = 0.05
v38K7 = 0.6	v38K7a = 0.0	v39K9 = 2.5	v40K5 = 20.0	v41J17 = 0.3
v41k17 = 10.0	v41k17a = 0.35	v42J1 = 0.1	v42K1 = 0.6	v42K1a = 0.1
v44K19 = 20.0	v44K19a = 0.0	cell = 1.0	A_k7 = 1e-08	A_k11 = 0.0556
A_k12 = 0.772	A_k13 = 0.02	A_k5 = 0.2	A_k6 = 0.01	A_k3 = 1.0
A_k4 = 1.0	A_k8 = 1e-04	A_k9 = 0.07	A_k10 = 0.001	A_k14 = 9.4e-04
A_k15 = 10.0	A_k16 = 9.5	A_k17 = 0.02	A_k16 = 6.0	A_k19 = 0.004
A_k20 = 0.005	A_k36 = 1e-05	A_k37 = 1e-04	A_k38 = 1e-06	k100 = 2.0
k101 = 1.0	k102 = 0.0	k103 = 1e-04	k104 = 0.07	k105 = 0.01
BeWe_v1b = 9.0	BeWe_k1b = 1.0	BeWe_k1i = 0.56	BeWe_c = 0.01	BeWe_ p = 8.0
BeWe_k1d = 0.12	BeWe_k2b = 0.3	BeWe_q = 2.0	BeWe_k2d = 0.05	BeWe_k2t = 0.24
BeWe_k3t = 0.02	BeWe_k3d = 0.12	BeWe_v4b = 3.6	BeWe_k4b = 2.16	BeWe_r = 3.0
BeWe_k4d = 0.75	BeWe_k5b = 0.24	BeWe_k5d = 0.06	BeWe_k5t = 0.45	BeWe_k6t = 0.06
BeWe_k6d = 0.12	BeWe_k6a = 0.09	BeWe_k7a = 0.003	BeWe_k7d = 0.09	

Conradie constants	Abroudi non-optimized constants	Novel constants	Geier constants

Table 1. Completed model constants. Constants taken from the Conradie model are shown in pink, while unscaled constants taken from the Abroudi model and novel empirically generated constants are shown in orange and yellow, respectively.

P27T = CA + CD + CE + P27
CYCAT = CA + CYCA
CYCD = CD + CYCD
CYCET = CE + CYCE
V8 = K8a + (K8 * (YB * CYCB + YE * (CYCA + CYCE))) / (CYCET + J8)
V6 = K6a + K6 * (HA * CYCA + HB * CYCB + HE * CYCE)
V4 = K4 * (GA * CYCA + GB * CYCB + GE * CYCE)
V2 = K2aa * CDc20 + K2a * (1 - CDh1) + K2 * CDh1
PP1A = PP1T / (1 + K21 * (FB * CYCB + FE * (CYCA + CYCE)))
DDS = 0.002 through 0.016
DSB = DDS * exp(-A_k7 * t)
DEG = A_k11 - A_k12 * (DSB - DDS * exp(-A_k13 * DDS * t))

Conradie algebraic equations	Abroudi algebraic equations

Table 2. Completed model algebraic equations. Equations taken from the Conradie model are shown in pink, while equations taken from the Abroudi model and adapted to the Conradie model are shown in orange.

v1 = v1k16 * ERG	v2 = v2k18 * DRG
v3 = K10 * CD	v4 = K10 * CYCD
v5 = K25 * CYCE * P27	v6 = K25 * CYCA * P27
v7 = v7k24 * CYCD * P27	v8 = v8k24r * CD
v9 = K30 * CDc20 * CYCA	v10 = K30 * CA * CDc20
v11 = K25R * CE	v12 = K25R * CA
v13 = V8 * CE	v14 = V8 * CYCE
v15 = V6 * P27	v16 = V6 * CE
v17 = V6 * CD	v18 = V6 * CA
v19 = V2 * CYCB	v20 = ((v20K3a + v20K3 * CDc20) * (1 - CDh1)) / (1 + v20J3 - CDh1)
v21 = (V4 * CDh1) / (v21J4 + CDh1)	v22 = v22K34 * PPX
v23 = (v23K31 * CYCB * (1 - IEP)) / (1 + v23J31 - IEP)	v24 = (v24K32 * IEP * PPX) / (v24J32 + IEP)
v25 = K12 * CDc20T	v26 = (v26K13 * (-CDc20 + CDc2-T) * IEP) / (v26J13 - CDc20 + CDc20T)
v27 = (v27K14 * CDc20) / (v27J14 + CDc20)	v28 = K12 * CDc20
v29 = K20 * (LA * CYCA + LB * CYCB + LD * (CD + CYCD) + LE * CYCE) * var5	v30 = K20 * (LA * CYCA + LB * CYCB + LD * (CD + CYCD) + LE * CYCE) * var 6
v31 = r31switch * v31K27 * MASS	v32 = v32K28 * GM
v33 = eps * v33MU * GM	v34 = (eps * v34k15) / (1 + DRG^2 / v34J15^2)
v35 = eps * (v35K11a + v35K11 * CYCB)	v36 = eps * v36K29 * MASS * var2
v37 = eps * v37K33	v38 = eps * (v38K7a + v38K7 * var2)
v39 = eps * v39K5 * DRG	v40 = eps * v40K5
v41 = eps * ((v41k17 * DRG^2) / (v41J17^2 * (1 + DRG^2 / v41J17^2)) + v41k17a * ERG)	v42 = eps * (v42K1a + (v42K1 * CYCB^2) / (v42J1^2 * (1 + CYCB^2 / v42J1^2)))
v43 = K20 * (LA * CYCA + LB * CYCB + LD * (CD + CYCD) + LE * CYCE) * var4	v44 = (PP1A * v44K15 + (-PP1A + PP1T) * v44K19a) * var1
v45 = K26R * var5	v46 = (K23a + K23 * (CYCA + CYCB)) * var2
v47 = K22 * var3	v48 = K26 * var2 * var4
v49 = K26R * var6	v50 = K26 * var3 * var4
v51 = K22 * var6	v52 = (K23a + K23 * (CYCA + CYCB)) * var5
v53 = A_k5 * DSB	v54 = A_k6 * ATM
v55 = A_k3 * aChk2	v56 = A_k4 * iChk2 * ATM
v57 = A_k8 + A_k10 * ATM	v58 = A_k10 * p53
v59 = DEG * Mdm2 * p53	v60 = A_k14 + tf * ((A_k15 * (IF)^50) / (A_k16)^50 + (IF)^50))
v61 = A_k17 * Mdm2	v62 = tf * (A_k18 * p53 * DSB) / (1 + A_k19 * p53 * Mdm2)
v63 = A_k20 * IF	v64 = A_k36 + A_k37 * p53
v65 = A_k38 * Gadd45a	v66 = k100 * var4
v67 = k101 * p16	v68 = k102 * p16
v69 = k103 * p21	v70 = k104 * p21
v71 = k105 * p53	v72 = (BeWe_v1b*(BeWe7 + BeWe_c)) / (BeWe_k1b*(1 + ((BeWe3/BeWe_k1l)^BeWe_p) + (BeWe7 + BeWe_c)))
v73 = BeWe_k1d*BeWe1	v74 = BeWe_k2b*(BeWe1^BeWe_q)
v75 = BeWe_k2d*BeWe2	v76 = BeWe_k2t*BeWe2
v77 = BeWe_k3t*BeWe3	v78 = BeWe_k3d*BeWe3
v79 = (BeWe_v4b*(BeWe3^BeWe_r))/((BeWe_k4b^BeWe_r)+(BeWe3^BeWe_r))	v80 = BeWe_k4d*BeWe4
v81= BeWe_k5b*BeWe4	v82 = BeWe_k5d*BeWe5
v83 = BeWe_k5t*BeWe5	v84 = BeWe_k6t*BeWe6
v85 = BeWe_k6d*BeWe6	v86 = BeWe_k7a*BeWe7
v87 = BeWe_k6a*BeWe6	v88 = BeWe_k7d*BeWe7
v89 = BeWe_k2b*BeWe6	

Conradie rate equations	Novel rate equations

Table 3. Completed model rate equations. Equations taken from the Conradie model are shown in pink, and novel empirically generated equations are shown in yellow.

CAp = v6 - v10 - v12 - v18	CDp = v7 - v3 - v8 - v17	CDc20p = v26 - v27 - v28
CDc20p = v26 - v27 - v28	CDc20Tp = v35 - v25	CDh1p = v20 - v21
CEp = v5 - v11 - v13 - v16	CYCAp = v12 + v18 + v36 + v67 + v69 + v6 - v9	CYCBp = v42 + v68 - v19
CYCDp = v8 + v17 + v39 - v4 - v7	CYCEp = v11 + 16 + v38 + v70 - v5 - v14	DRGp = v41 - v42
ERGp = v34 - v1	GMp = v31 - v32	IEPp = v23 - v24
MASSp = v33	PPXp = v37 - v22	var1p = v29 + v30 + v43 - v44
var2p = v29 + v45 + v47 - v46 - v48	var3p = v30 + v46 + v49 - v47 - v50	var4p = v44 + v45 + v49 - v43 - v48 - v50 - v66
var5p = v48 + v51 - v29 - v45 - v52	var6p = v50 + v52 - v30 - v49 - v51	P27p = v3 + v8 + v10 + v11 + v12 + v13 + v40 - v5 - v6 - v7 - v15
ATMp = v53 - v54	iChk2p = v55 - v56	aChk2p = v56 - v55
p53p = v57 - v58 - v59 - v71 -v89	Mdm2p = v60 - v61	IFp = v62 - v63
Gadd45ap = v64 - v65	p16p = v66 - v67 - v68	p21p = v71 - v69 - v70
BeWe1p = v72 - v73	BeWe2p = v74 - v75 - v76 + v77	BeWe3p = v76 - v77 - v78
BeWe4p = v79 - v80	BeWe5p = v81 - v82 - v83 + v84	BeWe6p = v83 - v84 - v85 + v86 - v87 - v71
BeWe7p = v87 - v86 - v88		

Conradie ODEs | Altered Conradie ODEs | Novel ODEs

Table 4. Completed model ODE equations. Equations taken from the Conradie model are shown in pink, while altered Conradie model equations and novel empirically generations are shown in blue and yellow, respectively.

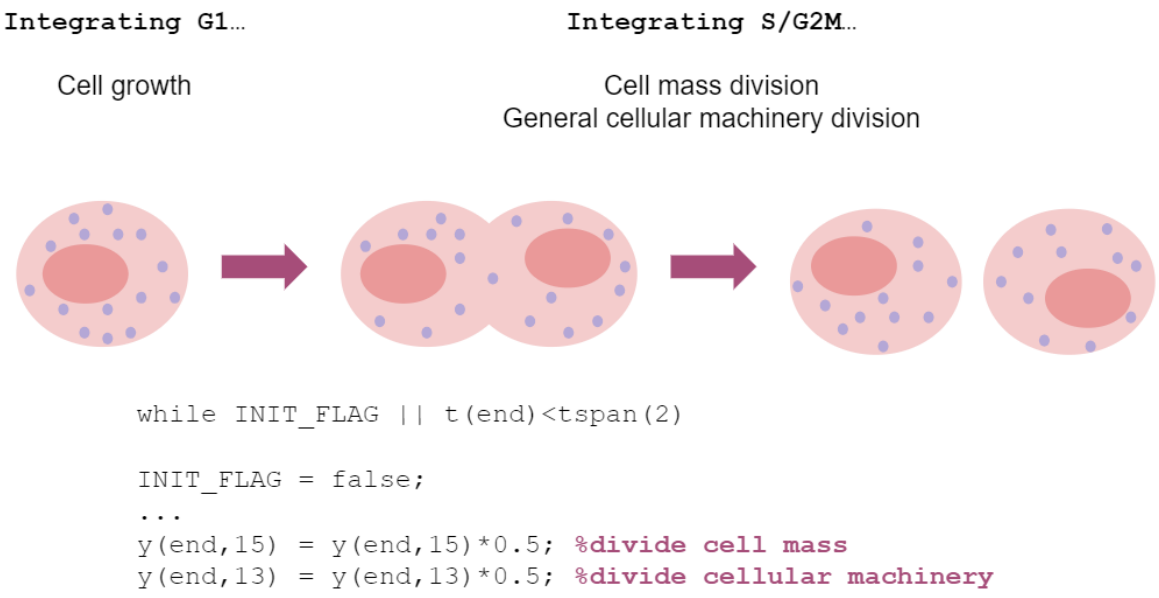

Figure 1. Mammalian cell division schematic accompanied by the corresponding MATLAB code segment.

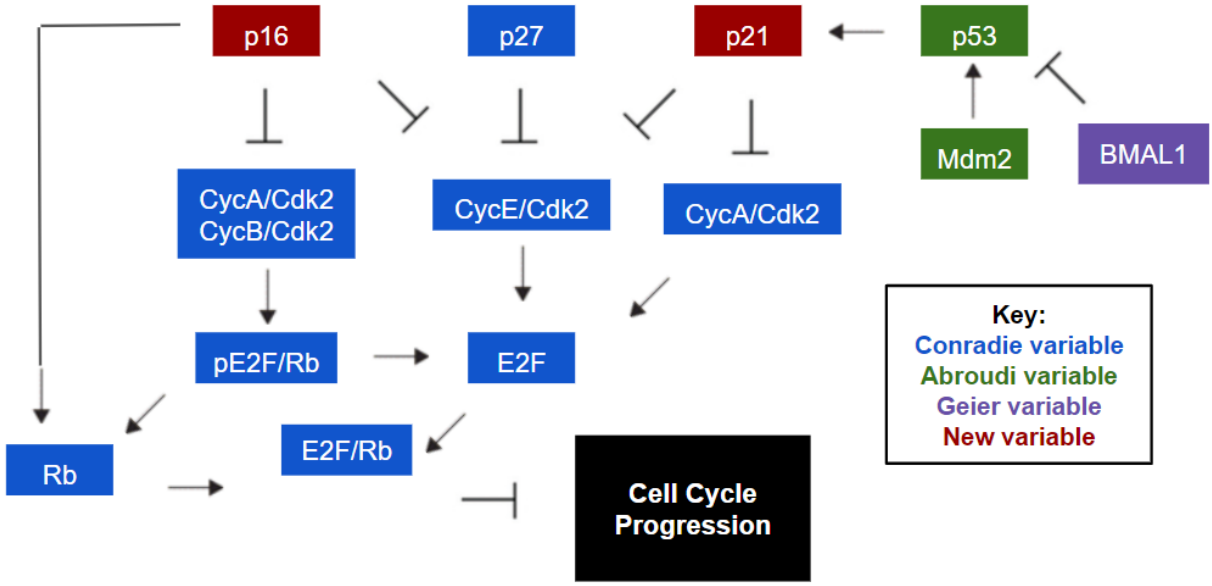

Figure 2. Proposed molecular signaling pathway combining integral DNA damage molecules from the Abroudi cell cycle model with the BMAL1 circadian rhythm module, omitted DNA damage proteins and key factors of the Conradie cell cycle model.

RESULTS

Cell Cycle Model Reconstruction and Optimization

The replication of the original Conradie model demonstrated reliable cyclical behavior over a period of 50 hours that is consistent with the molecular signaling pathways dominating the mammalian cell cycle, as shown in **Figure 3**. However, the absence of any modules accounting for the DNA damage stress response or circadian rhythm variation necessitated their integration for a comprehensive overview of the mammalian cell cycle as it pertains to quiescence and senescence.

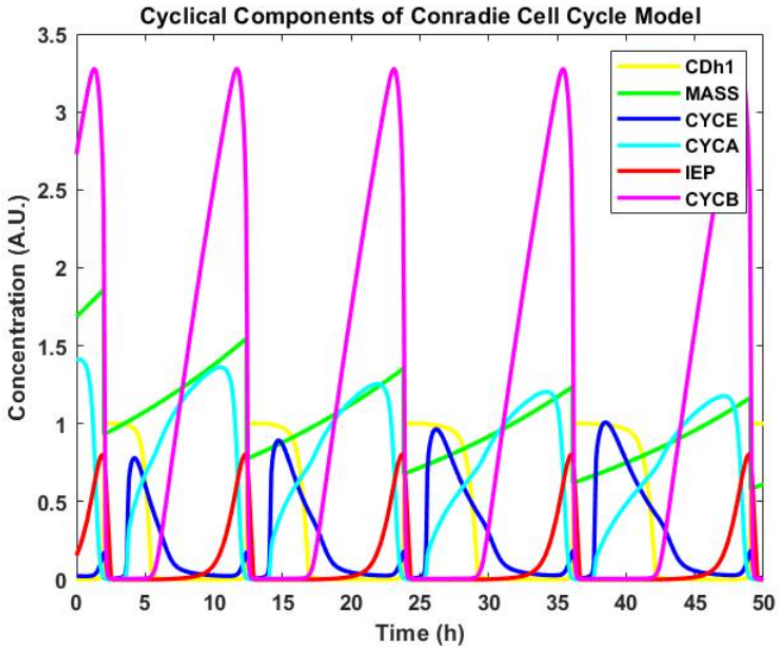

Figure 3. MATLAB-generated plot of the time course of the mammalian cell cycle, as replicated and optimized from the Conradie model.

Behavior of the novel integrated p53 DNA damage module was tested over a broad range of DNA damage input values, as shown in **Figure 4**. From these plots, it was observed that p53

expression rose exponentially before reaching a plateau phase under low (DDS = 0.002) and medium (DDS = 0.004) levels of input DNA damage. At high (DDS = 0.008) and excessive (DDS = 0.016) levels of DNA damage, the exponential growth phase was no longer observed and was replaced by rapid, repetitive cyclical behavior. These phenomena extend to the Mdm2 and IF molecules, both of which are key factors of the reconstructed and optimized p53 DNA damage module. These findings are in accordance with literary documentation of p53 behavior in

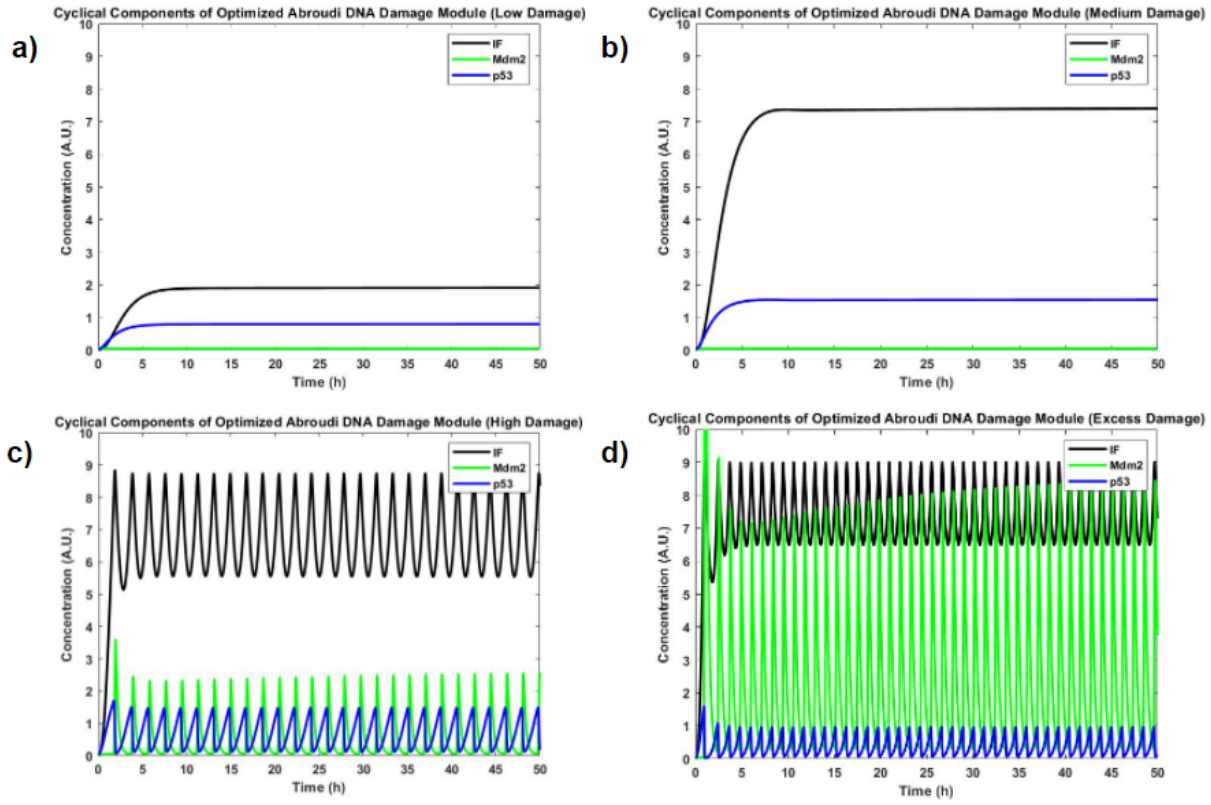

Figure 4. MATLAB-generated plots of the cyclical components of the optimized Abroudi DNA damage module under varying input levels of DNA damage stress (DDS), including **a)** low damage (DDS = 0.002); **b)** medium damage (DDS = 0.004); **c)** high damage (DDS = 0.008); and **d)** excess damage (DDS = 0.016).

response to DNA damage stress: under low stress conditions, DNA is capable of repair and the corresponding output is consistent with a faint pulse as observed in the figure. At higher levels of stress, the observed steady oscillations represent a combination of DNA damage repair and arrest of the cell cycle.[27]

Integration of the novel p16 module at a high (DDS = 0.008) level of input DNA damage is shown in **Figure 5**. The prolonged intervals between the cyclical events characterizing p16 behavior at this stage are consistent with literary documentation; however, there is no significant deviation from this pattern observed at lower levels of input DNA damage.[28] This inconsistency, in conjunction with a lack of significant impact of p16 protein on the behavior of the Cyclin A/Cdk2 and Cyclin B/Cdk2 complexes at such a high level of DNA damage, suggest insufficiency of one or more current constant values to model the delayed response of p16 and its

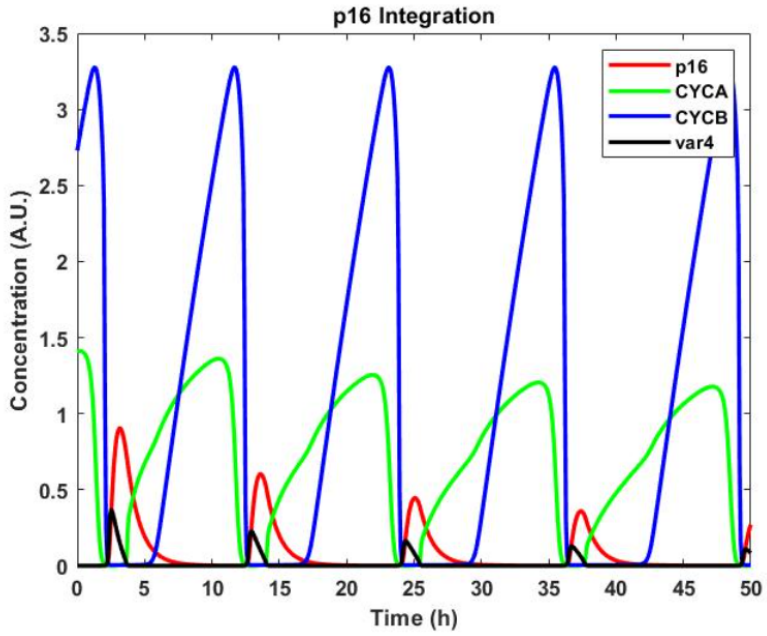

Figure 5. MATLAB-generated plot of the novel integration of p16 into the optimized Conradie-Abroudi cell cycle model.

effect on cell cycle function. In future iterations of this model, a systematic parameter variation will be conducted to refine these constant values.

The integration of the new p21 module over a broad range of DNA damage input values is shown in **Figure 6**. While exponential plot behavior was observed at low (DDS = 0.002) and medium (DDS = 0.004) levels of DNA damage, the exponential response was dampened and assumed a progressive embodiment of cyclical behavior at a high (DDS = 0.008) DNA damage level before stabilizing to a sustained, rapid cyclical pattern under excessive (DDS = 0.016) DNA damage. This model is consistent with experimental data of p21 protein behavior.[29] **Figure**

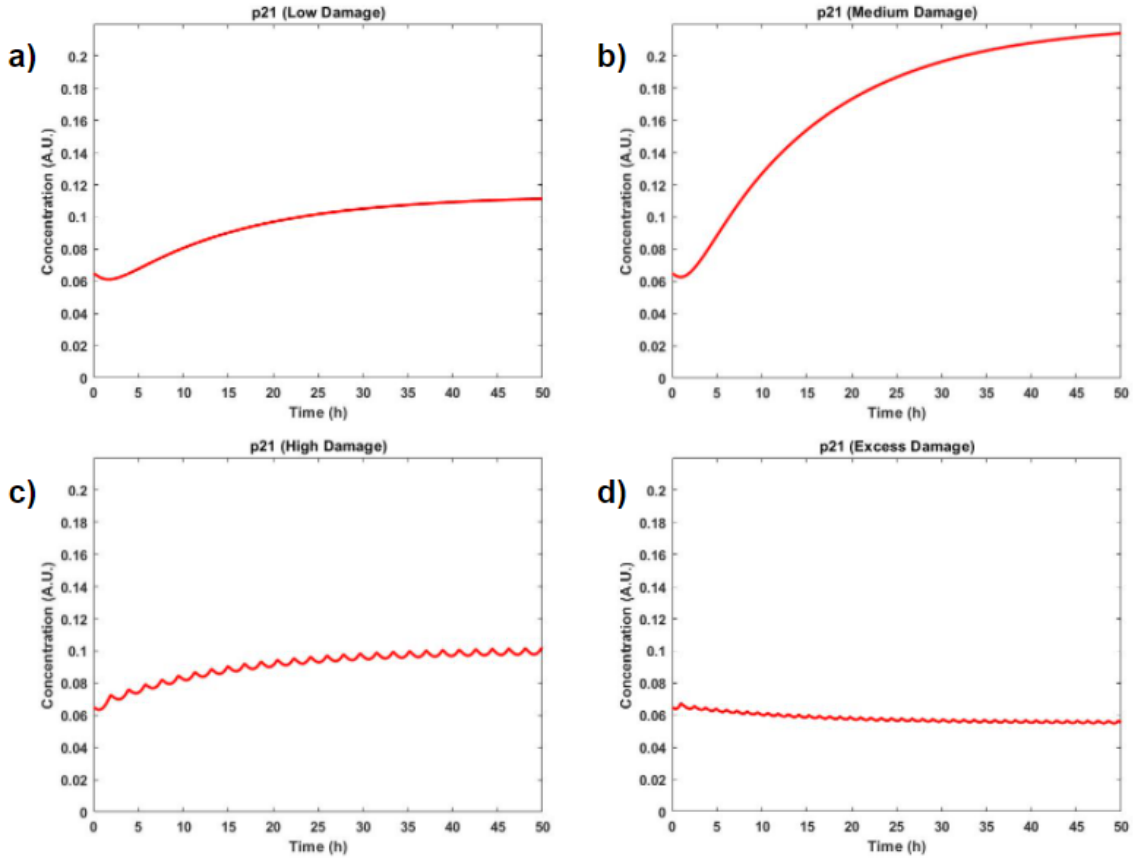

Figure 6. MATLAB-generated plot of the p21 molecule behavior under varying input levels of DNA damage stress (DDS), including **a)** low damage (DDS = 0.002); **b)** medium damage (DDS = 0.004); **c)** high damage (DDS = 0.008); and **d)** excess damage (DDS = 0.016).

7 further illustrates the success of this integration with the p53 DNA damage module. At all degrees of DNA damage, the plots of p21 and p53 closely mimic one another in terms of general behavior. At lower levels of DNA damage, both plots exhibit exponential trends that transition to plateaus after approximately five hours; similarly, both plots display rapid, cyclical behavior under higher applications of DNA damage stress. However, the absence of significant impact of

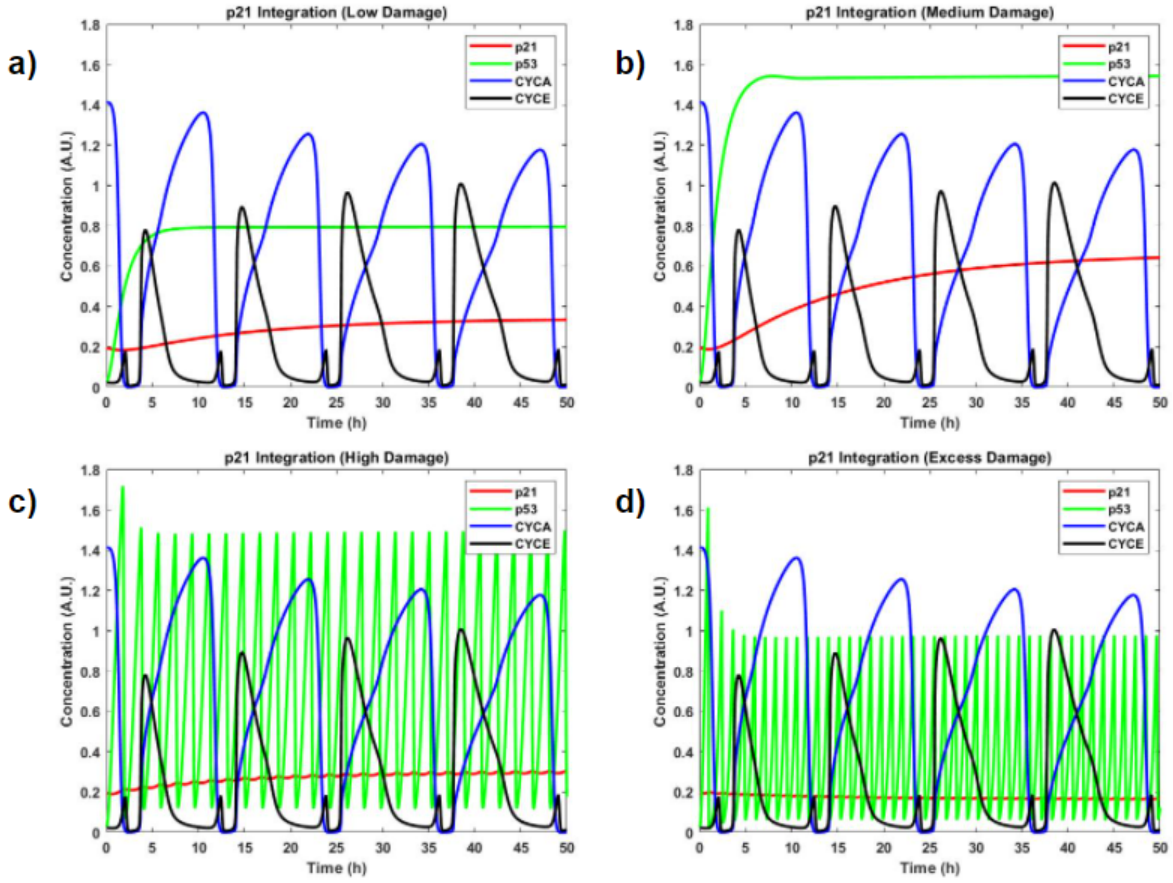

Figure 7. MATLAB-generated plot of the novel integration of p21 into the optimized Conradie-Abroudi cell cycle model under varying input levels of DNA damage stress (DDS), including **a)** low damage (DDS = 0.002); **b)** medium damage (DDS = 0.004); **c)** high damage (DDS = 0.008); and **d)** excess damage (DDS = 0.016).

p21 on the activity of the Cyclin A/Cdk2 and Cyclin E/Cdk2 complexes suggests that further constant refinement is needed via parameter variation in future iterations of this model.

The integration of the BMAL1 module over a broad range of DNA damage input values is shown in **Figure 8**. At low (DDS = 0.002) to medium (DDS = 0.004) levels of DNA damage, BMAL1 exhibited a dampening effect on the behavior of p53; however, this influence was significantly reduced at high (DDS = 0.008) to excessive (DDS = 0.016) levels of DNA damage.

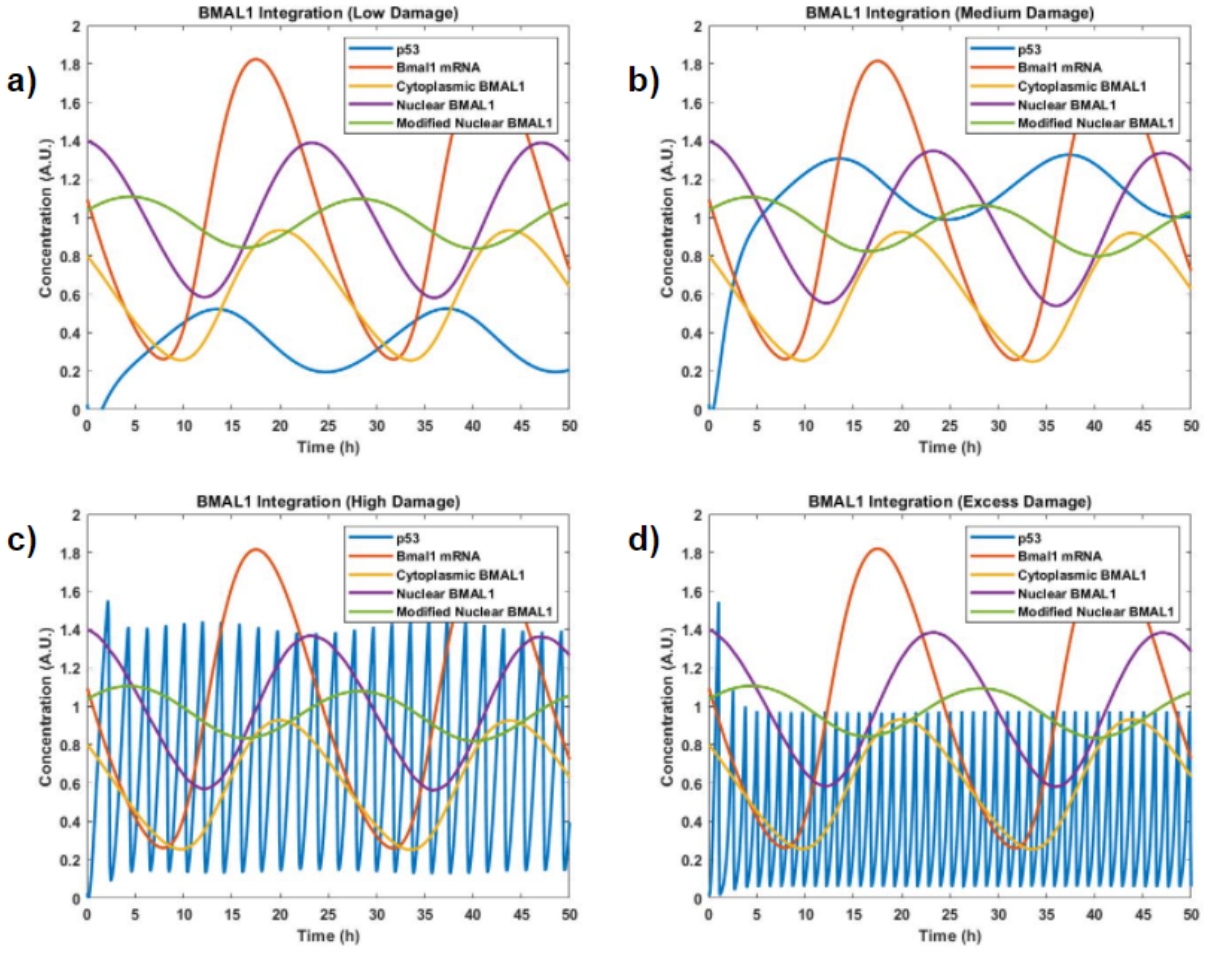

Figure 8. MATLAB-generated plot of the novel integration of BMAL1 into the optimized Conradie-Abroudi cell cycle model under varying input levels of DNA damage stress (DDS), including **a)** low damage (DDS = 0.002); **b)** medium damage (DDS = 0.004); **c)** high damage (DDS = 0.008); and **d)** excess damage (DDS = 0.016).

This model is consistent with experimental data of BMAL1 and p53 protein behavior.[26] However, this is a simplified overview of BMAL1 interaction with the cell cycle. While the model does account for the influence of cytoplasmic and nuclear PER and CRY protein complexes, there is no provision for the BMAL1/CLOCK complex; this heterodimer is a known positive regulator of circadian oscillation and Wee1, a nuclear protein that regulates cell cycle progression through inhibition of Cdk1.[30] These components will be incorporated in future iterations of this model to further elucidate the interactions between BMAL1 and key cell cycle regulators.

DISCUSSION

This work demonstrates the first documented attempt made to synthesize a computational model of the mammalian cycle that incorporates both circadian rhythm variation and a multi-faceted approach to the DNA damage response as coupled contributors to cycle regulation. As a preliminary step, a successful replication and optimization of an oscillating cell cycle model was executed. The integration of the novel p16 and p21 modules alongside the optimized p53 module allowed for the application of a range of DNA damage stress inputs to the system, with an output of senescence-associated protein behavior that simulated DNA damage repair events and cell cycle arrest at lower and higher stress input signals, respectively. Though this model behavior was particularly pronounced in both the p21 and p53 modules, expected p16 activity was only achieved at high levels of DNA damage stress. p16 also appeared to have a limited effect on cyclin dynamics, an observation that was inconsistent with experimental data and suggested the need for more sophisticated parameter selection. In future work, this will be accomplished through a screened comparison of constants in comparison to experimental observations using the approximate Bayesian computation sequential Monte Carlo (ABC-SMC) method. Further, integration of a circadian rhythm module featuring BMAL1 demonstrated the computational ability to restrict p53 behavior under limited DNA damage inputs; however, this module is constrained by simplification of the interactions between BMAL1 and cell cycle regulators, and will be expanded in future studies as complexity is added.

Following rectification of the aforementioned limitations to model function, several additions to this work will be explored to encompass a broader understanding of cell cycle regulation in response to circadian rhythm variation and DNA damage stress inputs. The current model plots molecular interactions over 50 hours, or slightly longer than two complete cell

cycles; future iterations of this model will extend this time period to 30 days to simulate a more relevant biological time scale of senescence-associated cell pathology. Further, DNA damage inputs will be adjusted to include tunable and time varying levels of DNA damage. To obtain a more detailed understanding of the interactions among circadian rhythm proteins, key cell cycle regulatory factors and DNA damage proteins, the repertoire of circadian proteins incorporated into this model will be expanded to include the 1- and 2- isoforms of period (PER) and cryptochrome (CRY) proteins. As previously noted for future parameter optimization, unknown rate constants will be screened using the ABC-SMC method.[31] Following these extensions, cell cycle arrest and senescence will be strategically simulated with an optimized DNA damage increase. Validation of the computational model of senescence will include cell cycle arrest stability after transient DNA damage stimuli, consistent with experimental data. When circadian rhythm and DNA damage modules have been satisfactorily expanded, model performance will be quantified through local sensitivity analyses of all system constants and initial conditions, including constants adapted from source mammalian cell cycle models. After these validations, this model will be integrated into a computational model of TM cell population dynamics to study the time course of glaucoma progression in both *in vitro* models and *in vivo* disease systems. Model performance will be cross-validated against *in vitro* experimental data of specific cell cycle and circadian rhythm components in TM cells, as well as published population and senescence studies of healthy and glaucomatous TM *in vivo*.

In summation, this project brings together vital molecular signaling components governing cellular growth and proliferation into one cohesive computational model. Of particular interest is the application of the base work demonstrated in this model to the development of a computational approach to the prediction and treatment of glaucoma pathology. Enhanced

understanding of the molecular signaling pathways implicated in glaucoma induction will enable future diagnostic and therapeutic developments, as identification of potential early markers of glaucoma progression, of which BMAL1 and p53 are of particular interest, may aid in preventative treatment to slow the progression of blindness in elderly populations. The development and further validation of this novel *in silico* framework of these molecular interactions will lead to an increasingly quantitative understanding of this disease; further, validation of BMAL1 as a key regulator of aging-associated diseases can be leveraged in future studies of other aging diseases and phenotypes.

WORKS CITED

1. Hunt, T., Nasymth, K., & Novak, B. (2011). The cell cycle. *Philosophical Transactions of the Royal Society of London, Series B, Biological Sciences, 366*(1584), 3494-3497. https://dx.doi.org/10.1098%2Frstb.2011.0274.
2. Ben-Porath, I., & Weinberg, R.A. (2005). The signals and pathways activating cellular senescence. *The international journal of biochemistry & cell biology, 37*(5), 961-976. https://doi.org/10.1016/j.biocel.2004.10.013.
3. Shariat, S.F., Tokunaga, H., Zhou, J., Kim, J., Ayala, G.E., Benedict, W.F., & Lerner, S.P. (2004). p53, p21, pRB, and p16 expression predict clinical outcome in cystectomy with bladder cancer. *Journal of Clinical Oncology, 22*(6), 1014-1024. https://doi.org/10.1200/jco.2004.03.118.
4. Terzi, M.Y., Izmirli, M., & Gogebakan, B. (2016). The cell fate: senescence or quiescence. *Molecular Biology Reports, 43*(11), 1213-1220. https://doi.org/10.1007/s11033-016-4065-0.
5. Huang, W., Ramsey, K., Marcheva, B., & Bass, J. (2011). Circadian rhythms, sleep, and metabolism. *Journal of Clinical Investigation, 121*(6), 2133-2141. https://doi.org/10.1172/JCI46043.
6. Refinetti, R., & Menaker, M. (1992). The Circadian Rhythm of Body Temperature. *Physiology & Behavior, 51*(3), 613-637. https://psycnet.apa.org/doi/10.1016/0031-9384(92)90188-8.
7. Takahashi, J. (2016). Molecular architecture of the circadian clock in mammals. *Research and Perspectives in Endocrine Interactions,* 13-24. http://dx.crossref.org/10.1007/978-3-319-27069-2_2.

8. Khapre, R.V., Kondratova, A.A., & Susova, O. (2011). Circadian clock protein BMAL1 regulates cellular senescence in vivo. *Cell Cycle, 10*(23), 4162-4169. https://dx.doi.org/10.4161%2Fcc.10.23.18381.
9. Abroudi, A., Samarasinghe, S., & D. Kulasiri. (2017). A comprehensive complex systems approach to the study and analysis of mammalian cell cycle control system in the presence of DNA damage stress. *Journal of Theoretical Biology, 429*(1), 204-228. https://doi.org/10.1016/j.jtbi.2017.06.018.
10. Conradie, R., Bruggeman, F.J., Ciliberto, A., Csikasz-Nagy, A., Novak, B., Westerhoff, H.V., & Snoep, J.L. (2009). Restriction point control of the mammalian cell cycle via the cyclin E/Cdk2:p27 complex. *The FEBS Journal, 277*(1), 357-367. https://doi.org/10.1111/j.1742-4658.2009.07473.x.
11. Iwamoto, K., Hamada, H., Eguchi, Y., & Okamoto, M. (2011). Mathematical modeling of cell cycle regulation in response to DNA damage: exploring mechanisms of cell-fate determination. *Biosystems, 103*(1), 384-391. https://doi.org/10.1016/j.biosystems.2010.11.011.
12. Weis, M.C., Avva, J., Jacobberger, J.W., & Sreenath, S.N. (2014). A Data-Driven, Mathematical Model of Mammalian Cell Cycle Regulation. *PLoS One, 9*(5), e97130. https://doi.org/10.1371/journal.pone.0097130.
13. Collado, M., Blasco, M.A., & Serrano, M. (2007). Cellular senescence in cancer and aging. *Cell, 130*(2), 223-233. https://doi.org/10.1016/j.cell.2007.07.003.
14. Hanoun, M., Eisele, L., Suzuki, M., Greally, J.M., Huttmann, A., Aydin, S., Scholtysik, R., Klein-Hitpass, L., Duhrsen, U., & Durig, J. (2012). Epigenetic silencing of the circadian clock gene CRY1 is associated with an indolent clinical course in chronic

lymphocytic leukemia. *PLoS One, 7*(3), e34347. https://doi.org/10.1371/journal.pone.0034347.

15. Jiang, W., Zhao, S., Jiang, X., Zhang, E., Hu, G., Hu, B., Zheng, P., Xiao, J., Lu, Z., Lu, Y., Ni, J., Chen, C., Wang, X., Yang, L., & Wan, R. (2016). The circadian clock gene Bmal1 acts as a potential anti-oncogene in pancreatic cancer by activating the p53 tumor suppressor pathway. *Cancer letters, 37*(2), 314-325. http://dx.doi.org/10.1016/j.canlet.2015.12.002.
16. Zeng, Z.L., Luo, H.Y., Yang, J., Wu, W.J., Chen, D.L., Huang, P., & Xu, R.H. (2014). Overexpression of the circadian clock gene Bmal1 increases sensitivity to oxaliplatin in colorectal cancer. *Clinical Cancer Research, 20*(4), 1042-1052. https://doi.org/10.1158/1078-0432.ccr-13-0171.
17. Trott, A.J., & Menet, J.S. (2018). Regulation of circadian clock transcriptional output by CLOCK:BMAL1. *PLoS Genetics, 14*(1), e1007156. https://doi.org/10.1371/journal.pgen.1007156.
18. Duffy, J.F., Zitting, K., & Chinoy, E.D. (2015). Aging and Circadian Rhythms. *Sleep Medicine Clinics, 10*(4), 423-424. https://dx.doi.org/10.1016%2Fj.jsmc.2015.08.002.
19. Ciulla, L., Moorthy, M., Mathew, S., Siesky, B., Verticchio Vercellin, A.C., Price, D., Januleviciene, I. & Harris, A. (2020). Circadian Rhythm and Glaucoma: What do We Know? *Journal of Glaucoma, 29*(2), 127-132. https://doi.org/10.1097/ijg.0000000000001402.
20. Raghunathan, V.K., Morgan, J.T., Park, S.A., Weber, D., Phinney, B.S., Murphy, C.J., & Russell, P. (2015). Dexamethasone Stiffens Trabecular Meshwork, Trabecular Meshwork

Cells, and Matrix. *Investigative Ophthalmology & Visual Science, 56*(8), 4447-4459. https://doi.org/10.1167/iovs.15-16739.

21. Geier, F., Becker-Weimann, S., Kramer, A., & Herzel, H. (2005). Entrainment in a model of the mammalian circadian oscillator. *Journal of Biological Rhythms, 20*(1), 83-93. https://doi.org/10.1177/0748730404269309.
22. Murray, A. (1994). Cell cycle checkpoints. *Current Opinion in Cell Biology, 6*(6), 872-876. https://doi.org/10.1016/0955-0674(94)90059-0.
23. Gartel, A.L., Serfas, M.S., & Tyner, A.L. (1996). p21 -- negative regulator of the cell cycle. *Proceedings of the Society for Experimental Biology and Medicine, 213*(2), 138-149. https://doi.org/10.3181/00379727-213-44046.
24. Park, K.J., & Soslow, R.A. (2020). Neoplastic Lesions of the Cervix. *Gynecologic Pathology (Second Edition)*, Elsevier, 227-293. https://doi.org/10.1016/B978-0-323-35909-2.00008-4.
25. He, G., Siddik, Z.H., Huang, Z., Wang, R., Koomen, J., Kobayashi, R., Khokhar, A.R., & Kuang, J. (2005). Induction of p21 by p53 following DNA damage inhibits both Cdk4 and Cdk2 activities. *Oncogene, 24*(18), 2929-2943. https://doi.org/10.1038/sj.onc.1208474.
26. Kawamura, G., Hattori, M., Takamatsu, K., Tsukada, T., Ninomiya, Y., Benjamin, I., Sassone-Corsi, P., Ozawa, T., & Tamaru, T. (2018). Cooperative interaction among BMAL1, HSF1, and p53 protects mammalian cells from UV stress. *Communications Biology, 22*(1), 204. https://doi.org/10.1038/s42003-018-0209-1.

27. Chong, K.H., Samarasinghe, S., & Kulasiri, D. (2015). Mathematical modelling of p53 basal dynamics and DNA damage response. *Mathematical Biosciences, 1*(1), 27-42. https://doi.org/10.1016/j.mbs.2014.10.010.

28. Kang, C., Xu, Q., Martin, T.D., Li, M.Z., Demaria, M., Aron, L., & Lu, T. (2015). The DNA damage response induces inflammation and senescence by inhibiting autophagy of GATA4. *Science, 349*(6255), aaa5612. https://doi.org/10.1126/science.aaa5612.

29. Karimian, A., Ahmadi, Y., & Yousefi, B. (2016). Multiple functions of p21 in cell cycle, apoptosis and transcriptional regulation after DNA damage. *DNA Repair, 42*(1), 63-71. https://doi.org/10.1016/j.dnarep.2016.04.008.

30. Tominaga, Y., Li, C., Wang, R., & Deng, C. (2006). Murine Wee1 plays a critical role in cell cycle regulation and pre-implantation stages of embryonic development. *International Journal of Biological Sciences, 2*(4), 161-170. https://doi.org/10.7150/ijbs.2.161.

31. Moral, P.D., Doucet, A., & Jasra, A. (2012). An adaptive sequential Monte Carlo method for approximate Bayesian computation. *Statistics and Computing, 22*(1), 1009-1020. https://doi.org/10.1007/s11222-011-9271-y.